Journal of Molecular Graphics and Modelling 44 (2013) 145–154

Contents lists available at SciVerse ScienceDirect

Journal of Molecular Graphics and Modelling

journal homepage: www.elsevier.com/locate/JMGM

Interactions of acetylcholine binding site residues contributing to nicotinic acetylcholine receptor gating: Role of residues Y93, Y190, K145 and D200

Prema L. Mallipeddi [a], Steen E. Pedersen [b,*], James M. Briggs [a,*]

[a] Department of Biology and Biochemistry, University of Houston, Houston, TX 77204, USA
[b] Department of Molecular Physiology and Biophysics, Baylor College of Medicine, Houston, TX 77030, USA

ARTICLE INFO

Article history:
Accepted 27 May 2013
Available online 15 June 2013

Keywords:
nAChR
Resting state
Desensitized state
αγ interface
αδ interface
Molecular dynamics

ABSTRACT

The nicotinic acetylcholine receptor exhibits multiple conformational states, resting (channel closed), active (channel open) and desensitized (channel closed). The resting state may be distinguished from the active and desensitized states by the orientation of loop C in the extracellular ligand binding domain (LBD). Homology modeling was used to generate structures of the *Torpedo californica* $\alpha_2\beta\delta\gamma$ nAChR that initially represent the resting state (loop C open) and the desensitized state (loop C closed). Molecular dynamics (MD) simulations were performed on the extracellular LBD on each nAChR conformational state, with and without the agonist anabaseine present in each binding site (the αγ and the αδ sites). Three MD simulations of 10 ns each were performed for each of the four conditions. Comparison of dynamics revealed that in the presence of agonist, loop C was drawn inward and attains a more stable conformation. Examination of side-chain interactions revealed that residue αY190 exhibited hydrogen-bonding interactions either with residue αY93 in the ligand binding site or with residue αK145 proximal to the binding site. αK145 also exhibited side chain (salt bridge) interactions with αD200 and main chain interactions with αY93. Residues αW149, αY198, γY116/δT119, γL118/δL121 and γL108/δL111 appear to play the role of stabilizing ligand in the binding site. In MD simulations for the desensitized state, the effect of ligand upon the interactions among αK145, αY190, and αY93 as well as ligand-hydrogen-bonding to αW149 were more pronounced at the αγ interface than at the αδ interface. Differences in affinity for the desensitized state were determined experimentally to be 10-fold. The changes in side chain interactions observed for the two conformations and induced by ligand support a model wherein hydrogen bond interactions between αD200 and αY93 are broken and rearrange to form a salt-bridge between αK145 and αD200 and hydrogen bond interactions between αY93 and αY190 and between αK145 and αY190.

© 2013 Elsevier Inc. All rights reserved.

1. Introduction

Nicotinic acetylcholine receptors (nAChRs) belong to the Cys-loop super family of ligand-gated ion-channels [1]. The muscle-type receptor initiates electrical signals in response to acetylcholine (ACh) release at the neuromuscular junctions followed by binding to nAChRs. Neuronal subtype receptors are known to mediate or modulate brain function such as learning, and memory; abnormal functioning of nAChRs is known to be involved in neuropsychiatric disorders [1–3].

The nAChR receptors are constituted of five pseudo-symmetrically arranged subunits, which can be homomeric or heteromeric ($\alpha_2\beta\delta\gamma$ or $\alpha_2\beta_3$ or α_5). The muscle type nicotinic acetylcholine receptor (nAChR) from the electric organ of *Torpedo marmorata* and *Torpedo californica* is a heteropentamer ($\alpha_2\beta\delta\gamma$) (Suppl. Fig. 1) [4,5]. nAChRs undergo conformational changes through at least three states: resting state (channel closed), active (channel open), and desensitized (channel closed) [6–9]. The *Torpedo* nAChR cryoelectron structure by Unwin [10] likely represents a resting state conformation of the receptor, with the loop C extended away from the binding interface. The acetylcholine binding protein (AChBP) has 20–24% sequence identity with the extracellular ligand-binding domain (LBD) of the nAChR and most of the conserved residues in the ligand binding sites of the nAChRs are present in AChBP [11]. The antagonist-bound and the apo-AChBP forms of the protein likely model the resting state of the nAChR [12,13] whereas crystal structures of AChBP in complex

Abbreviations: ACh, acetylcholine; nAChR, nicotinic acetylcholine receptor; AChBP, acetylcholine binding protein; LBD, ligand binding domain; dTC, *d*-tubocurarine; DC6C, Dansyl C6 Choline.

* Corresponding authors. Tel.: +1 713 743 8366; fax: +1 713 743 8351.
E-mail address: jbriggs@uh.edu (J.M. Briggs).

1093-3263/$ – see front matter © 2013 Elsevier Inc. All rights reserved.
http://dx.doi.org/10.1016/j.jmgm.2013.05.010

with agonists such as nicotine, carbamylcholine, and epibatidine [11,13,14] likely reflect the desensitized conformation [15] of the nAChR LBD. The desensitized state has the loop C aligned close to the binding site interfaces.

The *Torpedo* nAChR receptor has two agonist binding sites, one at the αγ-interface and the second at the αδ-interface (Suppl. Fig. 1) [16]. Each site comprises a set of conserved aromatic residues: on the α subunit, Y93 on loop A, W149 on loop B, Y190 and Y198 on loop C and, on the γ/δ complementary side, W54/57 [10]. The αγ and αδ sites exhibit distinct affinities for several antagonists (*d*-tubocurarine, α-conotoxin) and an agonist (epibatidine) [17–21], with preference typically toward the αγ interface. In contrast, the natural agonist, ACh, and its fluorescent analog dansyl-C6-choline (DC6C) exhibit slightly (3-fold) higher affinity for the αδ site in the desensitized state. This affinity difference is 100-fold in the resting state, with the affinity of the αδ site near 1 μM and the αγ site near 100 μM, both of which are substantially weaker than the nM affinity in the desensitized state [22]. This large affinity difference is important for the activation dose-response, which follows αγ site binding. In the AChBP, it has been shown that aromatic binding site residues are the first ones to undergo a closed to open structural change upon agonist binding [11,13,14]. Mutational studies, indicate that αW149, αY93 and αY190 coordinate as one unit in gating conformational changes [23]. Experimental [10,24,25] and computational [26–31] studies proposed various hypotheses as to how ligand binding triggers conformational changes in the loop C region that are transmitted to the transmembrane domain and ultimately cause channel gating. αD200 (strand β10) and αK145 (strand β7) are two residues close to the binding site and pair-wise mutations of Mukhtasimova et al. [25] indicate that an electrostatic interaction between these residues has a role in nAChR and channel gating. Mutation of αD200 alone also has been found to impair channel gating [32,33].

Anabaseine, a marine toxin, is known to activate both muscle and neuronal α7 nAChR subtypes [34]. A high resolution structure of the marine toxin anabaseine in complex with *Aplysia californica* AChBP shows that the mode of binding is similar to the agonists nicotine and epibatidine [35]. The benzylidene analogs of anabaseine are known to selectively bind to the α7 nAChR and one of the analogs, 3-(2,4-dimethoxybenzyliden)-anabaseine (DMXBA) is in clinical trials for treating schizophrenia [36,37]. We chose anabaseine as the ligand for our current studies because it is a medium sized agonist and the analogs are potential drug candidates.

To understand the role of side-chain interactions in the agonist binding site and its immediate vicinity, on nAChR gating, we carried out extensive molecular dynamics simulations in the absence and presence of anabaseine. We initiated the simulation from models of the nAChR in its resting and the desensitized states. The interactions between ligand binding site residues and ligand as well as the corresponding effects on the loop C region were also analyzed for distinct behavior at the αγ vs. the αδ agonist binding sites. The changes provide evidence for a re-arrangement of salt-bridge and hydrogen-bonding interactions during upon that likely provide the initial impetus for the gating conformational changes.

2. Materials and methods

2.1. Homology modeling

In order to generate structures of the extracellular ligand-binding domain of the nAChR for molecular dynamics studies, we used the *T. marmorata* nAChR as the basis structure to homology model the *T. californica* nAChR. This was important because our functional assays are routinely carried out using *T. californica*. *T. californica* has greater than 79% sequence identity to the *T. marmorata* nAChR and 23% sequence identity to AChBP. While the exact conformational state of the *T. marmorata* nAChR structure is unknown, the work on the AChBP strongly suggests that it represents the resting state of the receptor [13]. Structures of the AChBP have been determined in various agonists known to stabilize the desensitized state and have been determined in the presence of antagonists that stabilize the resting state [13,14,35]. To homology model the resting state, we simply used the *T. marmorata* structure. To model the desensitized state, we used the *T. marmorata* structure as the basis for the bulk of the nAChR, and also we used the AChBP in an agonist-bound conformation to model the binding site.

The ligand-binding domain of the *T. californica* nAChR was aligned with the *T. marmorata* nAChR sequence (PDBID 2BG9) [10]. The sequence alignment was based on the multi-sequence ClustalX [38] alignment as shown in Brejc, 2001 [11], to ensure correct alignment of sequentially conserved residues. The δ subunit has 14 residues poorly resolved and these residues were not included in building the homology model. All five subunits were modeled simultaneously using Modeller9v1 [39,40]. The "patch" command in Modeller was used to define the disulfide bonds. Structures were initially evaluated by PROCHECK [41] for residues with improper dihedral angles. Subsequently, the model was evaluated visually for proper side-chain dispositions paying close attention to the acetylcholine binding sites. Structures of nAChR (PDBID 2BG9), AChBP (PDBID UW6) and lysine scanning mutagenesis [42] studies were used for reference to check the homology model for misplaced residues. The homology model of the desensitized state was developed similarly, with the exception of the loop C region. In order to mimic the closed loop C, the region was modeled using both nAChR loop C as well as AChBP loop C regions as templates. The structures were subsequently refined by step-wise energy minimization using GROMACS 4.0.7 [43]. Step-wise energy minimization involved 4 steps: in step 1, all heavy atoms were fixed, then (step 2) only backbone atoms were fixed and then (step 3) Cα atoms were fixed. In the final step 4, unconstrained energy minimization was carried out. Minimization was carried out until the maximum force in each atom was less than100 kJ/mol nm.

2.2. Docking

Anabaseine was docked at the αγ and the αδ binding sites to the energy minimized resting state of nAChR using Autodock 4.2 [44]. AutoDockTools 1.5.4 was used in preparing the system [44]. A grid box with $56 \times 56 \times 56$ grid points at 0.375-Å spacing was prepared and centered at the loop C binding interface. Partial atomic charges were calculated using the Gasteiger method [45]. The Lamarckian Genetic Algorithm was used and the number of runs was set to 100. In each run, 300 randomly distributed conformations of anabaseine were evaluated. The number of energy evaluations was set to 2,500,000.

Docked poses with the lowest energy from each run were saved and clustered with an RMSD cut-off of 2 Å. The most populated cluster's conformation was chosen at each of the αγ and the αδ interfaces. The nAChR–anabaseine complex was then subjected to step-wise energy minimization as described earlier, using GROMACS 4.0.7 [43]. Two important hydrogen bonds are suggested based on the 2.7 Å resolution crystal structure of the AChBP–anabaseine complex [35]. One is a hydrogen bond between the protonated N1 on the ligand and the backbone carbonyl group of αW149 and the other is a bridged water molecule interaction between the pyridine N and the main chain atoms of residues γL118/δL121 and γL108/δL111. For comparison, the starting nAChR–anabaseine complex has the N1 of anabaseine facing the carbonyl oxygen of αW149 at both sites and the pyridine N at the αγ interface close to the carbonyl oxygen of γL117. The overall orientation of anabaseine at either interfaces is similar to that of

the AChBP–anabaseine crystal structure (PDBID 2WNL) [35]. The desensitized state anabaseine–nAChR complex was based on the resting state nAChR–anabaseine complex.

2.3. Molecular dynamics

The energy minimized unliganded-nAChR and the complexes with bound anabaseine were subjected to MD simulations using GROMACS 4.0.7 employing the GROMOS96 force field [43]. The topologies for ligand were generated by PRODRG server. Charges for the ligand were generated using the semi-empirical AM1-BCC method from antechamber [46]. For each simulation, the nAChR pentamer was immersed in a cubic box of SPC water [47] with at least 1.0 nm of water between the receptor and edges of box. 45 sodium ions were added to neutralize the system [48]. The N-terminus of the system was charged and the C terminus was kept neutral. This is because the extracellular domain C-terminus of the nAChR is directly linked to the transmembrane helices. To mimic the effect of terminal residues constrained by the transmembrane domain, the Cys loop that sits in between the four transmembrane helices (M1–M4), the direct peptide connection of loop C to M1 via β10 and the β1–β2 hairpin loop that associates the M2–M3 loop were restrained. MD simulations were carried out under periodic boundary conditions. An NTP ensemble with a Berendsen reference pressure of 1.0 bar and temperature 300 K was used [49]. The long range electrostatic interactions were computed by the Particle Mesh Ewald (PME) method [50]. 0.9 nm and 1.4 nm cut-offs were used for Coulomb and van der Waals interactions, respectively. The SHAKE algorithm [51] with a time-step of 2 fs was used to constrain bonds involving hydrogen atoms. Each system was gradually heated (10 K/ps gradient) from 0 to 300 K and then equilibrated for 2 ns. Subsequently, three separate 10 ns MD simulations were carried out (Suppl. Fig. 2). Each simulation had the same starting coordinates but different initial velocities to enhance conformational sampling and minimize bias from starting conditions [52,53].

2.4. Analysis of results

Simulations were analyzed every ps for distances, hydrogen-bonding interactions, and salt bridge interactions using the g_dist, g_saltbr and g_hbond programs from GROMACS [43]. The cut-off for salt-bridges was 4.0 Å between the oxygen atoms of acidic residues and the nitrogen atoms of basic residues. For hydrogen-bonds, we used a donor-acceptor distance cut-off of 3.5 Å and a donor-hydrogen-acceptor angle cut-off of 30°. In some cases we also used a simple 4 Å cutoff to identify hydrogen-bonding propensity. Secondary structure analysis was carried out on loop C residues (187–198) using the Timeline plugin in VMD 1.9.1 [54]; every 4th frame of the combined 30 ns trajectory for each system was used. Ligand-conformational clustering was carried out using the g_cluster module of GROMACS with a 2.0 Å cut-off. Interaction energies between selected residues and anabaseine were obtained using the g_energy analysis tool from GROMACS [43].

2.5. Fluorescence binding assay

nAChR-enriched membranes were obtained from *T. californica* electric organ (Aquatic Research Consultants, San Pedro, CA) as described previously [55,56]. DC6C was synthesized following the method of Walksman *et al.*, as described previously [57,58]. Proadifen (SKF-522) was purchased from Research Biochemical (Natick, MA); carbamylcholine was purchased from Sigma–Aldrich (St. Louis, MO). Fluorescence was measured using an SLM 8000C fluorometer with excitation light from a 350 W xenon short arc lamp, passed through an excitation monochromator and a UV-pass filter (Oriel 59152). Each sample was excited at a λ_{ex} of 295 nm at a bandwidth of 1.0 nm. Fluorescence emission was collected through 340 nm bandpass filter [22]. Binding of DC6C to the nAChR was measured as the change in the intensity of fluorescence due to energy transfer from protein aromatic residues [57]. Samples were typically 3 ml in stirred cuvettes in HTPS (pH 7.0) buffer (need reference) with competing ligands added sequentially by titration. Nonspecific fluorescence of DC6C was determined by including 1 mM carbamylcholine in parallel titrations.

2.6. Binding assay data analysis

The fluorescence data were fit to a two-site inhibition model using Sigmaplot (IBM) software:

$$F = \min + \frac{A_1}{1+(x/K_1)} + \frac{A_2}{1+(x/K_2)}$$

where F represents observed fluorescence intensity, K represents 50% inhibitory concentration (IC_{50}), x represents concentration of the compound, and min represents the minimum, background fluorescence amplitude. A_1 and A_2 represent the fluorescent amplitude of each binding component.

Dissociation constants at each site were determined from the inhibition constant

$$K_d = \frac{IC_{50}}{1+(DC6C/K_{DC6C})}$$

K_{DC6C} represents DC6C equilibrium binding constant. K_{DC6C} in presence of proadifen is 3 nM at αδ and 9 nM at αγ [22]. K_{DC6C} in the absence of proadifen for both of the sites (αγ and αδ) is 30 nM [22,59].

3. Results

3.1. αD200 interactions with binding site residues

In order to understand the mechanisms in the nAChR that initiate gating, we examined the molecular dynamics trajectories of the ligand binding domain in the absence and presence of an agonist, anabaseine. Homology models of the nAChR ligand binding domain were constructed to represent the resting and the desensitized state (see Section 2). Each of these conformational states were then subjected to MD simulation with anabaseine bound or not bound, for a total of four structurally distinct simulations. Each structure was subjected to three 10 ns MD simulations for a total of 30 ns each. The runs were subsequently analyzed for changes in salt bridge formation, hydrogen-bonding, and general motion of loop C within each of the two binding sites. The simulations indicate a pattern of changes that likely initiate gating within the nAChR.

3.2. αD200 interactions with αK145

A mutational study of human muscle nAChR proposed that a salt-bridge between αD200 and αK145 has a role in the nAChR receptor gating mechanism [25]. Other studies on adult mouse nAChR and human muscle nAChR showed that mutation of αD200 directly affects channel gating [32]. In addition, several crystal structures of AChBP and nAChR exhibit αK145 favorably placed to form a salt-bridge with αD200 [11]. A stable salt bridge was also observed in a targeted molecular dynamics study of human α7 nAChR [29]. We analyzed our MD runs for the presence of the αD200–αK145 salt bridge in the unliganded nAChR and the nAChR–anabaseine complex in both resting and the desensitized conformations (Fig. 1A and B). In each case, for both sites and conformations, addition of anabaseine increased fraction of time the residues were within salt-bridge distance. Overall, the

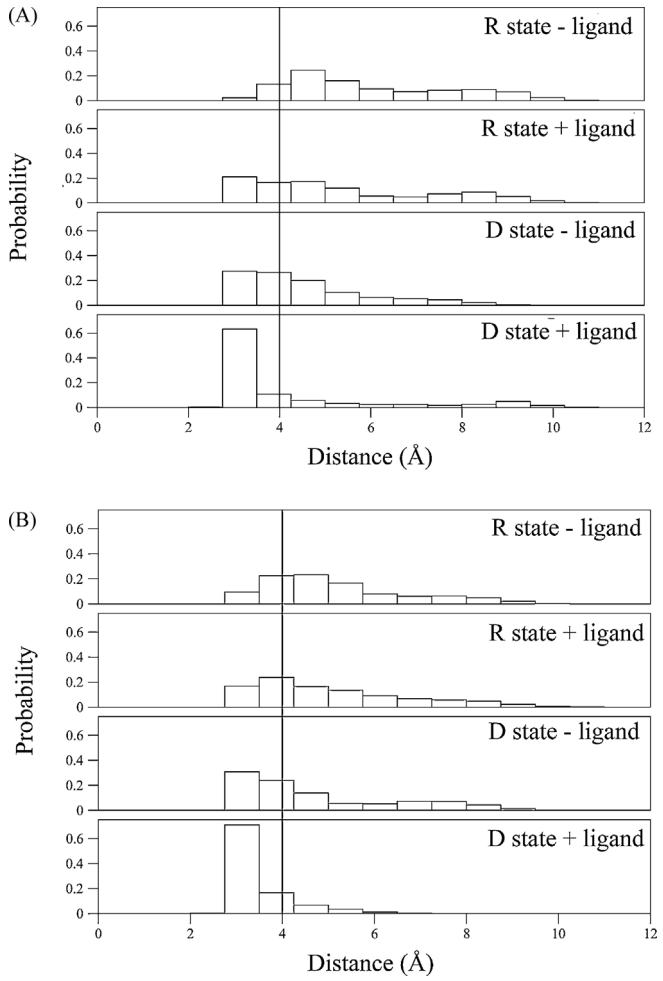

Fig. 1. The αK145(Nζ)–αD200(Cγ) salt-bridge is stabilized in the presence of ligand at the αγ and the αδ interfaces. The distances between these residues across the 30 ns MD simulations for the resting and desensitized states in the presence and absence of ligand are plotted as histograms. The line shows the cut-off distance. Panel A shows the distance distribution of nAChR at the αγ interface and panel B at the αδ interface. The percent of conformations exhibiting a salt-bridge at the αγ interface, resting state without ligand 11%, resting state with ligand 28%, desensitized state without ligand 43% and desensitized state with ligand 58%. At the αδ interface, the percent of conformations exhibiting a salt-bridge, resting state without ligand 24%, resting state with ligand 45%, desensitized state without ligand 47% and desensitized state with ligand 77%.

αK145–αD200 salt-bridge was substantially more prevalent in the desensitized state as compared to the resting state.

These observations, along with the prior experimental data, indicate that ligand binding induces the salt bridge between αD200 and αK145 and the bridge is also more pronounced in the desensitized state than in the resting state. Owing to the likely importance of αD200 to function, we analyzed other possible interactions, especially with the binding site residues αY93, αY190, αY198 and other proximal residues. At the resting-state αγ interface, αD200–αY93 hydrogen-bonding was observed for 80% of the trajectory (Fig. 2); this weakened in the presence of anabaseine (28%) and for the desensitized state, whether in the absence (24%) or presence (28%) of ligand. At the αδ interface, in the resting state with ligand, the trajectory exhibited 60% αD200–αY93 hydrogen-bonding that weakened to 27% in the desensitized state with ligand.

3.3. αY190 interactions with αK145

A targeted MD study based on a human α7 homology model, as well as an experimental mutation study on human muscle $\alpha_2\beta\delta\gamma$

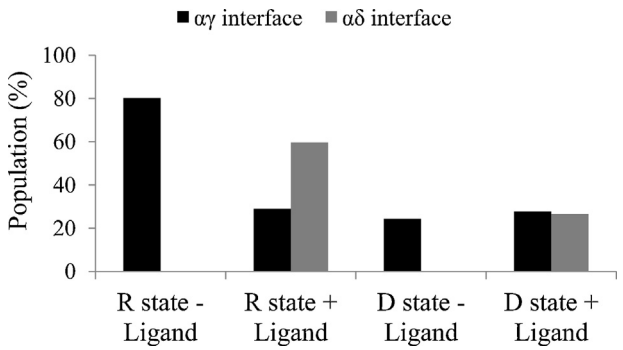

Fig. 2. The αD200 (Cγ)–αY93(OH) hydrogen-bonding was observed in the resting state. The percent of conformations exhibiting hydrogen-bonding at the αγ interface, resting state without ligand 80%, resting state with ligand 29%, desensitized state without ligand 24% and desensitized state with ligand 28%; at the αδ interface, resting state without ligand 0%, resting state with ligand 60%, desensitized state without ligand 0% and desensitized state with ligand 27%. No hydrogen-bonding was observed for the resting and desensitized states without ligand at the αδ interface.

nAChR, proposed an important role for the residues αK145 and αY190 in coupling agonist binding to gating [24,25]. We examined αY190 hydrogen-bonding interactions with αK145. In no case did these residues satisfy the 3.5 Å distance and the angle criteria for hydrogen-bonding. Using a simple 4 Å distance as a measure of hydrogen-bonding propensity, we found that only the desensitized state in the absence of ligand displayed a significant, albeit low, percentage of time within this distance (see Section 2 and Fig. 3A and B); 34% at the αγ interface and 15% at the αδ interface.

Because the interactions with αK145 are not particularly stable in the presence of ligand, we analyzed the MD simulations for other possible hydrogen-bonding interactions with residue αY190 that correlated with nAChR gating. Interactions between αY190 and αD200, αY198 or αY93 were analyzed; none were observed between αY190 and either αD200 or αY198. However, we did observe interactions with αY93 as described in the following section.

3.4. αY190 interactions with αY93

To evaluate hydrogen-bonding between αY93(OH) and αY190(OH) we used a simple distance criterion of 4 Å (Fig. 4A and B; indicated by the lines) between the oxygens. For the αγ interface, only the desensitized state in the presence of anabaseine exhibited a substantial percentage of the run within the cutoff distance. In contrast, the αδ site showed a substantial percentage in the presence of ligand for the resting state and 40–50% for the desensitized state. Overall the trend is toward a higher extent of H-bond formation in the desensitized state and in the presence of ligand. It is interesting here to note that the αK145–αY190 hydrogen-bonding is favored for the αγ interface in the unliganded desensitized state of nAChR (Fig. 3A).

The hydroxyl group of αTyr93 is in close contact with ligand, as observed from the X-ray crystal structures of AChBP with bound nicotine or epibatidine and the α7 nAChR with bound epibatidine [13,14,35,60]; the anabaseine-bound AChBP crystal structure also appears to have weak interactions between αTyr93 and the ligand [35]. Our observations, as well as prior experimental data suggest that ligand induces hydrogen-bonding interactions between αY93 and αY190 at the αγ interface.

Additionally, we also observed main chain hydrogen-bonding interactions between αK145 and αY93 for 67% of the trajectory at the αδ interface in the desensitized state with ligand, but not in the absence of ligand. At the αγ interface αK145–αY93 main chain hydrogen-bonding interactions were present for >75% of the

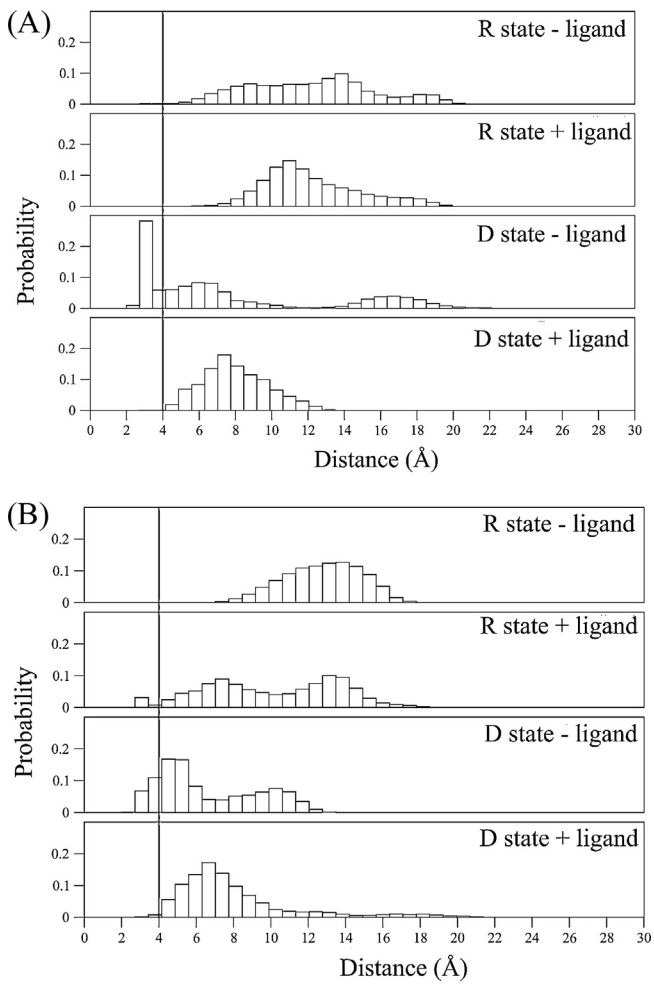

Fig. 3. The αK145 (Nζ)–αY190 (OH) hydrogen-bonding was prevalent in the desensitized state without ligand. Panel A shows the distance distribution of nAChR at the αγ interface and panel B at the αδ interface. A distance of <4.0 Å suggests a high probability for hydrogen-bonding interaction between αK145 and αY190. The percent of conformations exhibiting hydrogen-bonding at the αγ interface, resting state without ligand 0%, resting state with ligand 0%, desensitized state without ligand 34% and desensitized state with ligand 0%. At the αδ interface, the percent of conformations exhibiting hydrogen-bonding, resting state without ligand 0%, resting state with ligand 4%, desensitized state without ligand 15% and desensitized state with ligand 10%. The line reflects the 4 Å cut-off used to define the presence of hydrogen-bonding.

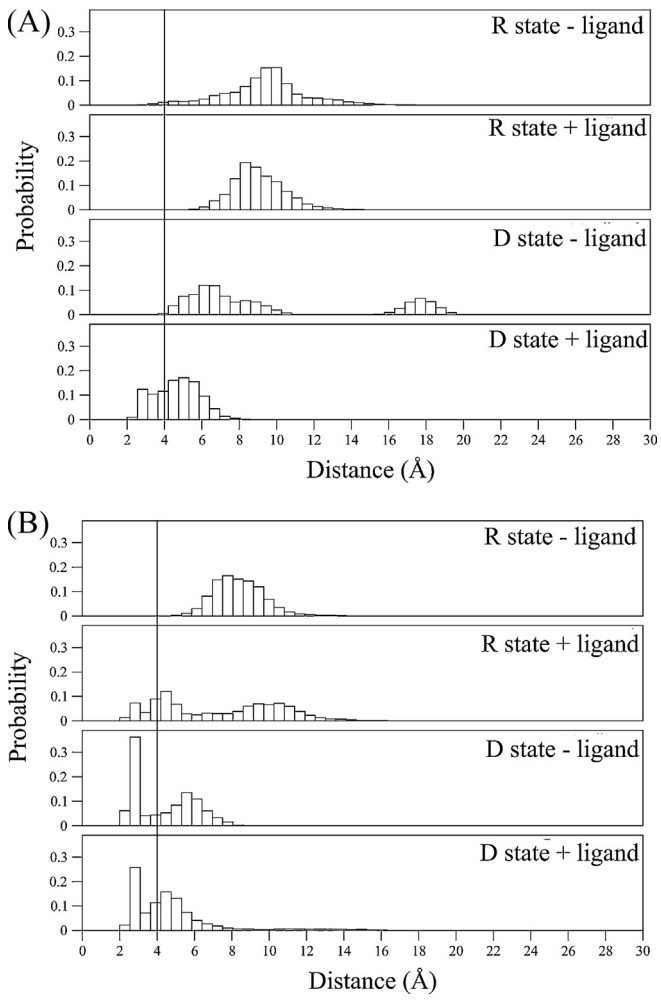

Fig. 4. The αY93(OH)–αY190(OH) distance distribution suggests hydrogen-bonding in the desensitized state, in the presence of ligand. The percent of conformations exhibiting a cut-off distance of less than 4.0 Å at the αγ interface (panel A) are as follows: resting state without ligand 0%, resting state with ligand 0%, desensitized state without ligand 0% and desensitized state with ligand 31%. At the αδ interface (panel B), the percentages are as follows: resting state without ligand 0%, resting state with ligand 17%, desensitized state without ligand 49% and desensitized state with ligand 41%.

trajectory in the presence of ligand for the resting state and irrespective of the presence or absence of ligand for the desensitized state (Suppl. Fig. 3).

3.5. Loop C conformations in the resting vs. desensitized states

NMR studies show that loop C exhibits multiple conformations in the absence of ACh as compared to the ACh-bound nAChR [61]. The AChBP crystal structures have Cα distances between residues equivalent to αC192 (loop C) and γW54/δW57 (loop B) of *T. californica* nAChR that vary from 15 to 18 Å, for various antagonist bound structures, whereas this distance is between 10 and 14 Å for agonist bound structures [10,13,14]. To examine the effect of ligand on the resting and desensitized nAChR loop C structures, the conformations were categorized based on this distance using 14 Å as a cutoff for classifying the loop as open or closed (see Fig. 5A and B).

For the resting state of nAChR in the absence of ligand, both at the αγ and the αδ interfaces, loop C is in the open state for more than 94% of the conformations (Fig. 5A and B). In the presence of anabaseine, the αδ interface has the loop C in the closed state 42% of the time whereas there is little effect at the αγ site. For the desensitized state, the loop C closed state is more prominent: greater than 41% of the conformations are closed at both the interfaces irrespective of the presence or absence of ligand. Furthermore, a trend toward an increase in the number of conformations with loop C in the closed state was observed in the presence of ligand at both of the interfaces (Fig. 5A and B) as well as smaller spreads in the distributions. Extended simulation runs might result in distinct loop C closed state conformations.

We carried out a secondary structure analysis of the loop C (residues 186–198) conformation (Fig. 6A and B). For the resting state without ligand loop C was of predominantly coil or turns as represented by orange and magenta regions at both the interfaces. Addition of ligand stabilizes loop C to some extent as observed by the appearance of blue and black regions representing beta sheet structure. This trend was more obvious for the desensitized state and upon addition of ligand. The αδ interface exhibited similar trends except for the desensitized state in the absence of ligand, which consisted mostly of coils turns and did

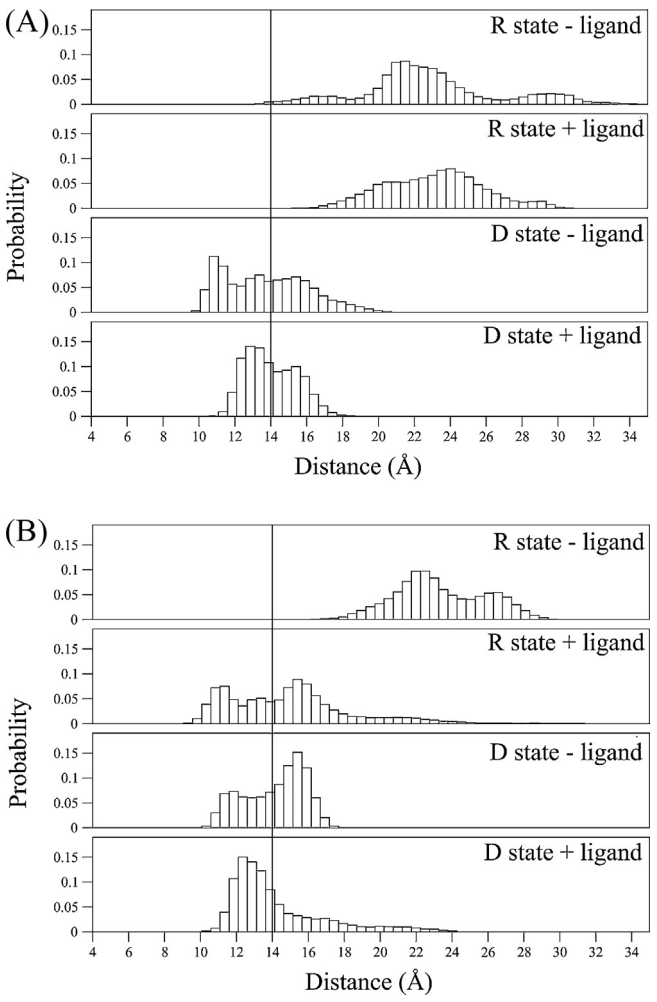

Fig. 5. Loop C closed state is stabilized upon ligand binding at the αγ (panel A) as well as the αδ interfaces (panel B). A cut-off distance of less than 14 Å between αCys192 (Cα) and γW54 (Cα) represents the loop C closed state. At the αγ interface, the percent of conformations exhibiting the loop C closed state in the resting state with ligand is 1% and without ligand it is 0%, the desensitized state without ligand is 55% and the desensitized state with ligand is 54%. At the αδ interface, the percent of conformations exhibiting the loop C closed state resting state without ligand is 0%, the resting state with ligand is 42%, the desensitized state without ligand is 41% and the desensitized state with ligand is 64%.

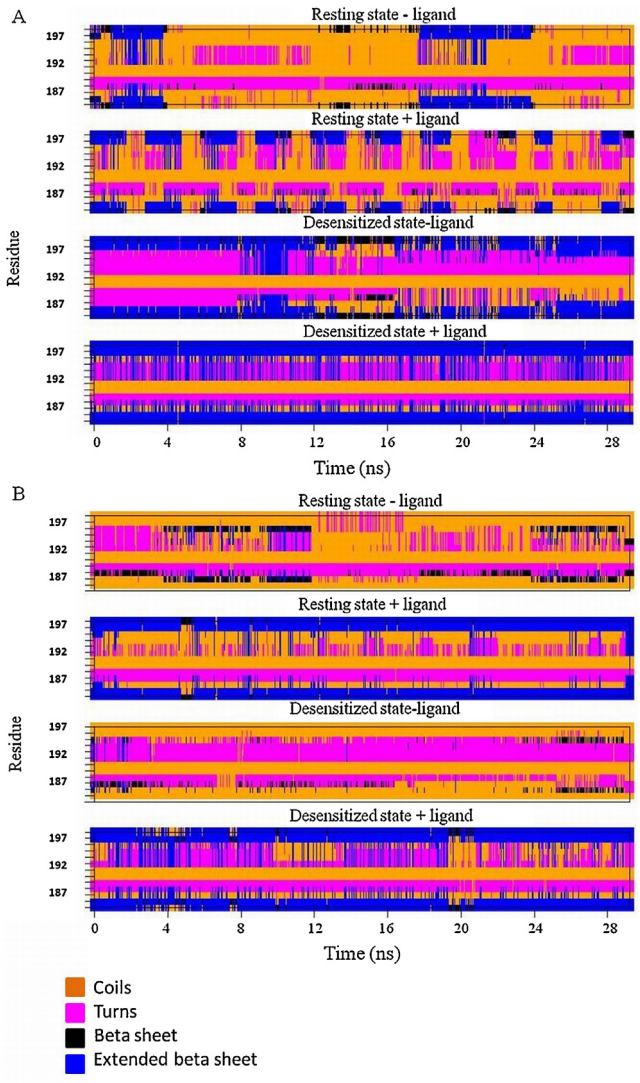

Fig. 6. Loop C attains a stable structure upon ligand binding for the desensitized state nAChR. Loop C secondary structure changes were monitored for the resting and desensitized states across the 30 ns trajectory at the αγ interface (A) and at the αδ interface (B). Loop C in the resting state predominantly exhibited coils and turns. The VMD timeline plugin was used to analyze the loop C (residues 187–198) secondary structure [54] and these are plotted as time vs. residue number.

not exhibit beta sheet nature. This analysis indicates more stable conformation in the presence of ligand than without ligand, for both resting and the desensitized states at both of the interfaces.

3.6. Ligand orientation and interactions

Ligand orientation and interactions were analyzed for the higher affinity, desensitized state in order to determine the primary ligand-stabilizing interactions. A hydrogen-bond is observed between the anabaseine N1 and the αW147(CO) for 70% of the trajectory at the αγ interface, while at the αδ interface, this was observed for only for 8%

of the trajectory (data not shown). Nevertheless, the anabaseine (N1)-αW149(CO) distance at the αδ interface was less than 4.0 Å for 92% of the trajectory. The positive charge on the ligand was believed to be compensated by equivalent hydrogen-bond interaction in agonist bound AChBP crystal structures [13,14,35].

The interaction energies between each of the binding site residues and anabaseine were calculated across the 30 ns trajectory in order to identify residues contributing to binding. Residues αW149 and αY198 contribute more to the interaction energy at both of the interfaces than other residues (Table 1). Anabaseine also exhibits favorable interactions with residues from the non-α subunit, γY116/δT119, γL118/δL121 and γL108/δL111.

Our observations agree with the crystal structure of anabaseine–AChBP complex, where equivalent interactions appeared to stabilize anabaseine [35].

The 2 Å crystal structure of anabaseine bound to AChBP reveals anabaseine bound in two distinct conformations [35]. They differ in the orientation of the tetrahydropyridine ring relative to the pyridine ring by a rotation of 90°. In one orientation, the N of the tetrahydropyridine ring (N1) faces the non-α subunit while in the second orientation, the N1 faces the α subunit. We observed a preference for the second orientation at the both interfaces (Fig. 7). A hydrogen-bonding interaction involving a bridged water molecule, the pyridine N of nAChR agonist and the main chains of γL118/δL121 or γL108/δL111 was proposed from the crystal structures of AChBP complexes [14,62]. We did not observe the role of any such bridging water molecule, in our simulations.

Table 1
Interaction energies (kJ/mol) between anabaseine and selected binding site residues.

	αγ interface		αδ interface	
	Coulomb energy	Lennard–Jones energy	Coulomb energy	Lennard–Jones energy
αY93	−0.0	−2.6	0.0	−1.5
αW149	−30.2	−15.8	−18.9	−18.4
γ/δW54	0.5	−1.9	0.3	−2.0
γY116/δT119	−1.7	−13.5	−3.4	−5.9
γL118/δL121	−0.9	−7.2	−3.9	−10.5
γL108/δL111	−0.2	−4.5	0.4	−8.2
αY190	−0.2	−4.9	−0.1	−3.8
αY198	−6.1	−11.6	−1.9	−5.7
Total mean interaction energy	−48.7	−97.3	−36.1	−87.0

3.7. Distinct behavior of the two ACh binding sites

The interactions between the conserved residues at the αγ interface were distinct from those at the αδ interface for the desensitized state of nAChR. αY190 exhibited hydrogen-bonding interactions with αK145 (36%) in the absence of anabaseine at the αγ interface, but these were less frequent (15%) at the αδ interface. The αY190–αY93 hydrogen-bonding was observed (>41%) irrespective of the presence or absence of anabaseine at the αδ interface, but at the αγ interface this was observed only in the presence of anabaseine (31%). Also, anabaseine exhibits stable hydrogen-bonding interactions with αW149 (70%) at the αγ interface but only for 8% of the time at the αδ interface. Furthermore, interaction energy calculations reveal more favorable interactions between anabaseine at the αγ relative to the αδ interface (Table 1).

In summary, loop C of the αδ interface is predisposed to the closed state and as the ligand binds, αY190 establishes stable contacts either with αK145 or αY93 or both. This reinforces the loop C closed state conformation. On the other hand, at the αγ interface, ligand binding induces loop C closure favoring hydrogen-bonding interaction between αY190 and αK145 or αY93. These observations are consistent with a weaker resting-state affinity at the αγ site and a larger change in agonist affinity from resting and desensitized states, as is observed for ACh and for DC6C [22]. Furthermore, anabaseine only exhibits a stable hydrogen-bond with αW149 at the αγ interface. Thus, each interface exhibited different conformational states on the time scale of our simulations and reflects differences in the behavior of the αγ vs. the αδ binding sites. Further studies involving longer simulation runs will provide clear insights into the stable conformation state, each of these interfaces might adopt.

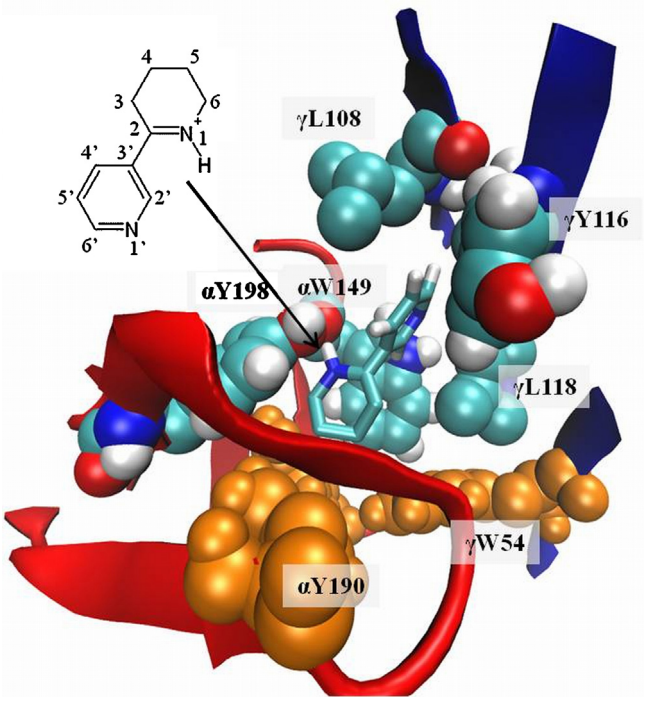

Fig. 7. Binding pose of anabaseine at the αγ interface. Binding site residues are shown in van der Waals representation and anabaseine is in stick form. Residues exhibiting most favorable interactions with the ligand are colored by atom type. Other residues in the binding site are colored orange.

3.8. Anabaseine binds with higher affinity to the αγ binding site vs. the αδ binding site

To determine whether the computationally determined anabaseine binding differences between the sites are reflected in their binding constants, we carried out fluorescence-based competitive binding assays using DC6C. Increasing concentrations of anabaseine were titrated into *Torpedo* nAChR rich membranes, equilibrated with 20 nM DC6C. Quenching of fluorescence indicated competitive displacement of DC6C from ACh binding sites. The resulting curve (Suppl. Fig. 4) fitted a two-site model and suggested distinct binding affinities of anabaseine to the αγ vs. the αδ ACh binding sites with K_1 = 0.03 μM and K_2 = 1.12 μM (Table 2).

To determine the correspondence between the two affinities and the two sites, titration experiments were carried out in the

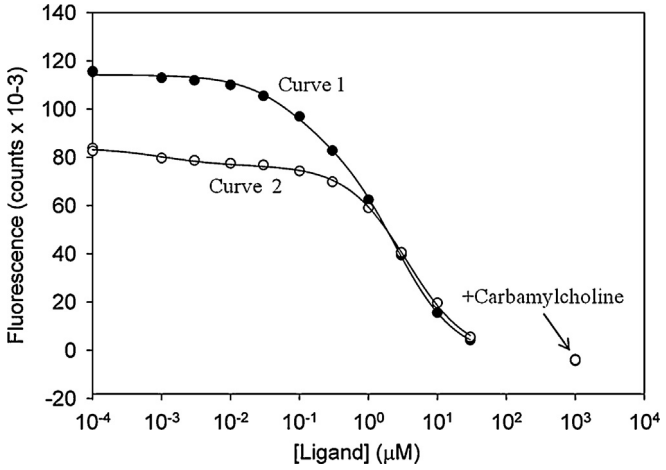

Fig. 8. Anabaseine binds with higher affinity to the αγ site than the αδ site. AChR-rich membranes (40 nM ACh binding sites) in HTPS were pre-incubated with DC6C (100 nM) and 10 μM proadifen in the presence or absence of 1 μM tubocurarine. Titrations were carried out with increasing concentrations of anabaseine. Five independent experiments were performed in the absence or presence of 1 mM carbamylcholine, with a λ_{ex} of 295 nm, as described in Section 2. Titration data were fit to a two-site inhibition model. For anabaseine in the presence of *d*-tubocurarine, K_1 = 0.002 and K_2 = 3.23 and in the absence of *d*-tubocurarine K_1 = 0.08 and K_2 = 2.56.

Table 2
Difference in the extent of binding in the presence and absence of tubocurarine. K_D values are calculated from fitted IC_{50} values. K_1 and K_2 values represent mean calculated from independent experiments ($n = 5$ for proadifen and $n = 3$ for no proadifen) and the standard error of mean is shown in parentheses.

	A_1 (AU)	A_2 (AU)	K_1 (μM)	K_2 (μM)	K_{D1} (μM)	K_{D2} (μM)
No proadifen	40 (3.4)	45 (0.3)	0.03 (0.006)	1.12 (0.10)	0.01	0.3
Proadifen	25 (5.4)	77 (5.5)	0.08 (0.008)	2.56 (0.07)	0.007	0.07
Proadifen + *d*TC	11 (2.4)	70 (2.8)	0.002 (0.001)	3.23 (0.10)	NS	0.09

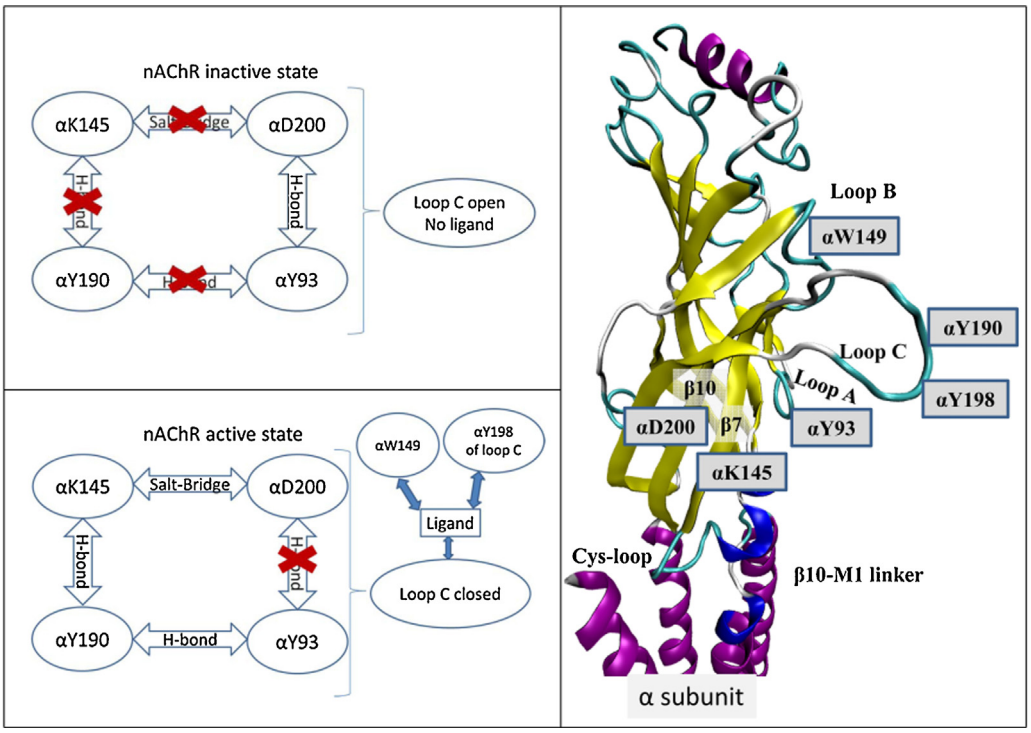

Fig. 9. Schematic representation of interactions among conserved residues in the nAChR active vs. the inactive state. nAChR in the inactive state has the loop C open and no significant interactions were observed among the residues αK145, αD200, αY190 and αY93. Ligand binding induces loop C closure and establishes interactions between residues αK145 and αD200, residues αY190 and αK145 or αY93. The resulting rearrangement of loops A, B, C strands β7 and β10 are proposed to be propagated to the channel via Cys-loop, β10-M1 linker and trigger channel opening.

presence of proadifen, to induce the high-affinity, desensitized state of the nAChR (Fig. 8). Two parallel experiments were performed, one in the absence and one in the presence of 1 μM *d*-tubocurarine, which specifically binds to the αγ site with higher affinity. In the absence of tubocurarine, fitting the specific binding curve to a two-site model resulted in 30-fold differences in the observed inhibition constants for the two sites, $K_1 = 2.6$ and $K_2 = 0.08$. The amplitudes in the absence of proadifen reflect the differences fluorescence yield at the two sites. The specific decrease in the amplitude of the higher affinity component by the presence of d-tubocurarine and, shows that it corresponds to the αγ site (Table 2). The residual observed binding corresponds to the αδ binding site. This data reveals anabaseine has higher affinity site for the αγ than the αδ binding site (Table 2). The anabaseine K_D values were computed from the observed *K*s and the known K_D values for the binding of DC6C at each site; they are also given in Table 2 and display a 10-fold affinity difference.

4. Conclusions

MD simulation studies on resting and desensitized states of nAChR with and without ligand (30 ns each) enabled us to understand how fluctuations at the ligand binding site bring about changes in the regions proximal to the binding site. Anabaseine is stabilized in the binding site by hydrogen-bonding, electrostatic and van der Waals interactions with residues contributing from both α and non-α subunits. Protein-ligand interaction energies shows that the ligand is stabilized by interaction with αW149 on loop B and αY190 and αY198 on loop C. Comparison of resting and desensitized states shows inward movements of loop C in the presence of ligand. This stabilizes hydrogen-bonding interactions between αY190 on loop C and either αY93 on loop A or αK145 on strand β7. Ligand-binding also favors αK145–αD200 salt-bridge formation, which coordinates motions between β7 and β10. Experimental binding assays showed that anabaseine binds to the αγ binding site with higher affinity (ca. 10×) than to the αδ binding site. Both experimental and computational studies reveal the αγ interface has distinct behavior as compared to the αδ interface.

The crystal structures of the AChBP and the human α7 nAChR have equivalent residues oriented favorably for hydrogen-bonding [13,14,35,60]. Other studies also indicate hydrogen-bonding between αK145(Nζ)–αY190(OH) [24,25] in the presence of ligand. However, we do not observe consistent hydrogen-bonding in our simulations. Our observations are consistent with a 15 ns MD study on an ACh bound α7 nAChR homology model wherein the homologous residue distances were always >6 Å [26] apart. However, weak hydrogen-bonding interaction between this pair was observed in a targeted MD study based on human α7 homology model [30]. Experimentally, mutation of both of these residues reduced channel gating but did not abolish it completely [25]. Based on current

MD simulations along with prior studies, we conclude that αK145 and αY190 have weak hydrogen-bonding interactions only in the desensitized state.

Loop C is closely packed in all of the agonist (nicotine, carbamylcholine, epibatidine and anabaseine) bound AChBP crystal structures [13,14,35,60] and NMR structures [61]. It is encouraging that our observations also agree well with the recently published high resolution X-ray structure of human α7 nAChR [60]. Although our results are inconsistent with an MD study on ACh-α7 nAChR simulations, where the loop C is observed to move outward in the presence of ACh, the authors of that study attributed this observation to insufficient sampling time [26].

Based on our observations we propose the following model (Fig. 9). In the inactive or resting state loop C stays away from the binding site. In the active state or the desensitized state, binding of ligand induces loop C closure. This brings αY190 closer to the binding site, which forms hydrogen-bonding interactions with αY93 or αK145 or with both. This further contributes to loop C in closed form as well as coordination of motions between loop C, loop A and strand β7. αK145 also forms stable salt-bridge interactions with αD200, which links β7 and β10 strand. This weakens hydrogen-bonding interactions between αY93 and αD200. αK145 also exhibits main chain hydrogen-bonding interactions with αY93 and acts to coordinate loops A and β7. Interactions with αY198 and αW149 stabilizes ligand, while coupling loop C and loop B. Overall, binding of ligand initiates loop C closure, induces interactions among the residues in and around binding site. Coordinated motions between loops A, B, C, strands β7 and β10. This, initiated at the two ACh binding sites, likely constitute the initial trigger motion that is transmitted to the transmembrane domain and resulting in channel opening.

αY93, by virtue of its proximity to loop-B and by interacting with residues on strand β10, β7 and loop C, potentially plays a crucial role in transmitting motions in the binding site to regions proximal to the binding site. It would be interesting to study pairwise mutations of αY93 vs. αD200, αK145 and αY190. All of the aromatic binding site residues are conserved among the *Torpedo* $\alpha_2\beta\delta\gamma$, α4β2, and α7 nAChRs. Thus, ligand induced conformational changes observed in $\alpha_2\beta\delta\gamma$ nAChR provides insights into these other sites. The current study provides valuable information for structure-based drug design efforts that selectively target nAChR subtypes. Future work including transmembrane domain and longer molecular dynamic simulations will provide better understanding of the gating mechanism involving loop C closure and opening of the channel.

Conflicts of interest

The authors are aware of no conflicts of interest in relation to the work described herein.

Acknowledgements

The authors would like to thank Dr. Tsai-wei Shen, Dr. Nagakumar Bharatham and Dr. Haimei Zhu for helpful discussions. We acknowledge Texas Learning and Computation Center and UH Information Technology Research Computing at the University of Houston for computational resources. This work was supported by a grant to SEP from the Dan L. Duncan Cancer Center at Baylor College of Medicine.

Appendix A. Supplementary data

Supplementary data associated with this article can be found, in the online version, at http://dx.doi.org/10.1016/j.jmgm.2013.05.010.

References

[1] H.A. Lester, M.I. Dibas, D.S. Dahan, J.F. Leite, D.A. Dougherty, Cys-loop receptors: new twists and turns, Trends in Neurosciences 27 (2004) 329–336.
[2] E.J. Hohnadel, C.M. Hernandez, D.A. Gearhart, A.V. Terry Jr., Effect of repeated nicotine exposure on high-affinity nicotinic acetylcholine receptor density in spontaneously hypertensive rats, Neuroscience Letters 382 (2005) 158–163.
[3] M. Quik, Smoking, nicotine and Parkinson's disease, Trends in Neurosciences 27 (2004) 561–568.
[4] M.A. Raftery, M.W. Hunkapiller, C.D. Strader, L.E. Hood, Acetylcholine receptor: complex of homologous subunits, Science 208 (1980) 1454–1456.
[5] M. Noda, H. Takahashi, T. Tanabe, M. Toyosato, S. Kikyotani, Y. Furutani, et al., Structural homology of *Torpedo californica* acetylcholine receptor subunits, Nature 302 (1983) 528–532.
[6] A. Karlin, Emerging structure of the nicotinic acetylcholine receptors, Nature Reviews Neuroscience 3 (2002) 102–114.
[7] A. Auerbach, G. Akk, Desensitization of mouse nicotinic acetylcholine receptor channels. A two-gate mechanism, Journal of General Physiology 112 (1998) 181–197.
[8] M.I. Schimerlik, U. Quast, M.A. Raftery, Ligand-induced changes in membrane-bound acetylcholine receptor observed by ethidium fluorescence. 3. Stopped-flow studies with histrionicotoxin, Biochemistry 18 (1979) 1902–1906.
[9] T. Heidmann, J.P. Changeux, Fast kinetic studies on the allosteric interactions between acetylcholine receptor and local anesthetic binding sites, European Journal of Biochemistry 94 (1979) 281–296.
[10] N. Unwin, Refined structure of the nicotinic acetylcholine receptor at 4A resolution, Journal of Molecular Biology 346 (2005) 967–989.
[11] K. Brejc, W.J. van Dijk, R.V. Klaassen, M. Schuurmans, J. van Der Oost, A.B. Smit, et al., Crystal structure of an ACh-binding protein reveals the ligand-binding domain of nicotinic receptors, Nature 411 (2001) 269–276.
[12] Y. Bourne, T.T. Talley, S.B. Hansen, P. Taylor, P. Marchot, Crystal structure of a Cbtx–AChBP complex reveals essential interactions between snake alpha-neurotoxins and nicotinic receptors, EMBO Journal 24 (2005) 1512–1522.
[13] S.B. Hansen, G. Sulzenbacher, T. Huxford, P. Marchot, P. Taylor, Y. Bourne, Structures of aplysia AChBP complexes with nicotinic agonists and antagonists reveal distinctive binding interfaces and conformations, EMBO Journal 24 (2005) 3635–3646.
[14] P.H. Celie, S.E. van Rossum-Fikkert, W.J. van Dijk, K. Brejc, A.B. Smit, T.K. Sixma, Nicotine and carbamylcholine binding to nicotinic acetylcholine receptors as studied in AChBP crystal structures, Neuron 41 (2004) 907–914.
[15] T. Grutter, J.P. Changeux, Nicotinic receptors in wonderland, Trends in Biochemical Sciences 26 (2001) 459–463.
[16] S.E. Pedersen, J.B. Cohen, d-Tubocurarine binding sites are located at alpha-gamma and alpha-delta subunit interfaces of the nicotinic acetylcholine receptor, Proceedings of the National Academy of Sciences of the United States of America 87 (1990) 2785–2789.
[17] R.J. Prince, S.M. Sine, Epibatidine binds with unique site and state selectivity to muscle nicotinic acetylcholine receptors, Journal of Biological Chemistry 273 (1998) 7843–7849.
[18] S.M. Sine, H.J. Kreienkamp, N. Bren, R. Maeda, P. Taylor, Molecular dissection of subunit interfaces in the acetylcholine receptor: identification of determinants of alpha-conotoxin M1 selectivity, Neuron 15 (1995) 205–211.
[19] R.V. Papineni, J.U. Sanchez, K. Baksi, I.U. Willcockson, S.E. Pedersen, Site-specific charge interactions of alpha-conotoxin MI with the nicotinic acetylcholine receptor, Journal of Biological Chemistry 276 (2001) 23589–23598.
[20] I.E. Andreeva, S. Nirthanan, J.B. Cohen, S.E. Pedersen, Site specificity of agonist-induced opening and desensitization of the *Torpedo californica* nicotinic acetylcholine receptor, Biochemistry 45 (2006) 195–204.
[21] R.M. Hann, O.R. Pagan, V.A. Eterovic, The alpha-conotoxins GI and MI distinguish between the nicotinic acetylcholine receptor agonist sites while SI does not, Biochemistry 33 (1994) 14058–14063.
[22] X.Z. Song, I.E. Andreeva, S.E. Pedersen, Site-selective agonist binding to the nicotinic acetylcholine receptor from *Torpedo californica*, Biochemistry 42 (2003) 4197–4207.
[23] J. Chen, Y. Zhang, G. Akk, S. Sine, A. Auerbach, Activation kinetics of recombinant mouse nicotinic acetylcholine receptors: mutations of alpha-subunit tyrosine 190 affect both binding and gating, Biophysical Journal 69 (1995) 849–859.
[24] F. Gao, N. Bren, T.P. Burghardt, S. Hansen, R.H. Henchman, P. Taylor, et al., Agonist-mediated conformational changes in acetylcholine-binding protein revealed by simulation and intrinsic tryptophan fluorescence, Journal of Biological Chemistry 280 (2005) 8443–8451.
[25] N. Mukhtasimova, C. Free, S.M. Sine, Initial coupling of binding to gating mediated by conserved residues in the muscle nicotinic receptor, Journal of General Physiology 126 (2005) 23–39.
[26] R.H. Henchman, H.L. Wang, S.M. Sine, P. Taylor, J.A. McCammon, Ligand-induced conformational change in the alpha7 nicotinic receptor ligand binding domain, Biophysical Journal 88 (2005) 2564–2576.

[27] R.H. Henchman, H.L. Wang, S.M. Sine, P. Taylor, J.A. McCammon, Asymmetric structural motions of the homomeric alpha7 nicotinic receptor ligand binding domain revealed by molecular dynamics simulation, Biophysical Journal 85 (2003) 3007–3018.
[28] R.J. Law, R.H. Henchman, J.A. McCammon, A gating mechanism proposed from a simulation of a human alpha7 nicotinic acetylcholine receptor, Proceedings of the National Academy of Sciences of the United States of America 102 (2005) 6813–6818.
[29] X. Liu, Y. Xu, H. Li, X. Wang, H. Jiang, F.J. Barrantes, Mechanics of channel gating of the nicotinic acetylcholine receptor, PLoS Computational Biology 4 (2008) e19.
[30] X. Cheng, H. Wang, B. Grant, S.M. Sine, J.A. McCammon, Targeted molecular dynamics study of C-loop closure and channel gating in nicotinic receptors, PLoS Computational Biology 2 (2006) e134.
[31] X. Cheng, I. Ivanov, H. Wang, S.M. Sine, J.A. McCammon, Nanosecond-timescale conformational dynamics of the human alpha7 nicotinic acetylcholine receptor, Biophysical Journal 93 (2007) 2622–2634.
[32] M.E. O'Leary, M.M. White, Mutational analysis of ligand-induced activation of the Torpedo acetylcholine receptor, Journal of Biological Chemistry 267 (1992) 8360–8365.
[33] G. Akk, S. Sine, A. Auerbach, Binding sites contribute unequally to the gating of mouse nicotinic alpha D200N acetylcholine receptors, Journal of Physiology 496 (Pt 1) (1996) 185–196.
[34] W.R. Kem, V.M. Mahnir, R.L. Papke, C.J. Lingle, Anabaseine is a potent agonist on muscle and neuronal alpha-bungarotoxin-sensitive nicotinic receptors, Journal of Pharmacology and Experimental Therapeutics 283 (1997) 979–992.
[35] R.E. Hibbs, G. Sulzenbacher, J. Shi, T.T. Talley, S. Conrod, W.R. Kem, et al., Structural determinants for interaction of partial agonists with acetylcholine binding protein and neuronal alpha7 nicotinic acetylcholine receptor, EMBO Journal 28 (2009) 3040–3051.
[36] A. Olincy, J.G. Harris, L.L. Johnson, V. Pender, S. Kongs, D. Allensworth, et al., Proof-of-concept trial of an alpha7 nicotinic agonist in schizophrenia, Archives of General Psychiatry 63 (2006) 630–638.
[37] R. Freedman, A. Olincy, R.W. Buchanan, J.G. Harris, J.M. Gold, L. Johnson, et al., Initial phase 2 trial of a nicotinic agonist in schizophrenia, American Journal of Psychiatry 165 (2008) 1040–1047.
[38] J.D. Thompson, T.J. Gibson, F. Plewniak, F. Jeanmougin, D.G. Higgins, The CLUSTAL_X windows interface: flexible strategies for multiple sequence alignment aided by quality analysis tools, Nucleic Acids Research 25 (1997) 4876–4882.
[39] N. Eswar, B. Webb, M.A. Marti-Renom, M.S. Madhusudhan, D. Eramian, M.Y. Shen, et al., Comparative protein structure modeling using Modeller, Current Protocols in Bioinformatics (2006) (Chapter 5, Unit 5.6).
[40] A. Sali, L. Potterton, F. Yuan, H. van Vlijmen, M. Karplus, Evaluation of comparative protein modeling by MODELLER, Proteins 23 (1995) 318–326.
[41] R.A. Laskowski, M.W. Macarthur, D.S. Moss, J.M. Thornton, Procheck – a program to check the stereochemical quality of protein structures, Journal of Applied Crystallography 26 (1993) 283–291.
[42] S.M. Sine, H.L. Wang, N. Bren, Lysine scanning mutagenesis delineates structural model of the nicotinic receptor ligand binding domain, Journal of Biological Chemistry 277 (2002) 29210–29223.
[43] D. Van Der Spoel, E. Lindahl, B. Hess, G. Groenhof, A.E. Mark, H.J. Berendsen, GROMACS: fast, flexible, and free, Journal of Computational Chemistry 26 (2005) 1701–1718.
[44] G.M. Morris, R. Huey, W. Lindstrom, M.F. Sanner, R.K. Belew, D.S. Goodsell, et al., AutoDock4 and AutoDockTools4: automated docking with selective receptor flexibility, Journal of Computational Chemistry 30 (2009) 2785–2791.
[45] J. Gasteiger, M. Marsili, Iterative partial equalization of orbital electronegativity – a rapid access to atomic charges, Tetrahedron 36 (1980) 3219–3228.
[46] J. Wang, W. Wang, P.A. Kollman, D.A. Case, Automatic atom type and bond type perception in molecular mechanical calculations, Journal of Molecular Graphics and Modelling 25 (2006) 247–260.
[47] H.C.J.P.M.P. Berendsen, W.F. van Gunsteren, J. Hermans, Interaction models for water in relation to protein hydration, Intermolecular Forces 33 (1981) 1–42.
[48] C. Oostenbrink, A. Villa, A.E. Mark, W.F. van Gunsteren, A biomolecular force field based on the free enthalpy of hydration and solvation: the GROMOS force-field parameter sets 53A5 and 53A6, Journal of Computational Chemistry 25 (2004) 1656–1676.
[49] H.J.C. Berendsen, J.P.M. Postma, W.F. Vangunsteren, A. Dinola, J.R. Haak, Molecular-dynamics with coupling to an external bath, Journal of Chemical Physics 81 (1984) 3684–3690.
[50] U. Essmann, L. Perera, M. Berkowitz, T. Darden, H. Leee, L. Pedersen, A smooth particle mesh Ewald method, Journal of Chemical Physics 103 (1995) 8577–8593.
[51] J.-P. Ryckaert, G. Ciccotti, H.J.C. Berendsen, Numerical integration of the cartesian equations of motion of a system with constraints: molecular dynamics of n-alkanes, Journal of Computational Physics 23 (1977) 327–341.
[52] A. Elofsson, L. Nilsson, How consistent are molecular dynamics simulations? Comparing structure and dynamics in reduced and oxidized *Escherichia coli* thioredoxin, Journal of Molecular Biology 233 (1993) 766–780.
[53] L.S. Caves, J.D. Evanseck, M. Karplus, Locally accessible conformations of proteins: multiple molecular dynamics simulations of crambin, Protein Science 7 (1998) 649–666.
[54] W. Humphrey, A. Dalke, K. Schulten, VMD: visual molecular dynamics, Journal of Molecular Graphics 14 (1996), 33–38, 27–28.
[55] S.E. Pedersen, R.V. Papineni, Interaction of d-tubocurarine analogs with the Torpedo nicotinic acetylcholine receptor. Methylation and stereoisomerization affect site-selective competitive binding and binding to the noncompetitive site, Journal of Biological Chemistry 270 (1995) 31141–31150.
[56] S.E. Pedersen, E.B. Dreyer, J.B. Cohen, Location of ligand-binding sites on the nicotinic acetylcholine receptor alpha-subunit, Journal of Biological Chemistry 261 (1986) 13735–13743.
[57] G. Waksman, M.C. Fournie-Zaluski, B. Roques, Synthesis of fluorescent acylcholines with agonistic properties: pharmacological activity on Electrophorus electroplaque and interaction in vitro with Torpedo receptor-rich membrane fragments, FEBS Letters 67 (1976) 335–342.
[58] X.Z. Song, S.E. Pedersen, Electrostatic interactions regulate desensitization of the nicotinic acetylcholine receptor, Biophysical Journal 78 (2000) 1324–1334.
[59] N.D. Boyd, J.B. Cohen, Desensitization of membrane-bound Torpedo acetylcholine receptor by amine noncompetitive antagonists and aliphatic alcohols: studies of [3H]acetylcholine binding and 22Na+ ion fluxes, Biochemistry 23 (1984) 4023–4033.
[60] S.X. Li, S. Huang, N. Bren, K. Noridomi, C.D. Dellisanti, S.M. Sine, et al., Ligand-binding domain of an alpha7-nicotinic receptor chimera and its complex with agonist, Nature Neuroscience 14 (2011) 1253–1259.
[61] F. Gao, G. Mer, M. Tonelli, S.B. Hansen, T.P. Burghardt, P. Taylor, et al., Solution NMR of acetylcholine binding protein reveals agonist-mediated conformational change of the C-loop, Molecular Pharmacology 70 (2006) 1230–1235.
[62] T.T. Talley, M. Harel, R.E. Hibbs, Z. Radic, M. Tomizawa, J.E. Casida, et al., Atomic interactions of neonicotinoid agonists with AChBP: molecular recognition of the distinctive electronegative pharmacophore, Proceedings of the National Academy of Sciences of the United States of America 105 (2008) 7606–7611.